FMRP REGULATES POSTNATAL NEURONAL MIGRATION VIA MAP1B

S. Messaoudi, J. Stoufflet, C. Fouquet, M. Doulazmi, A. Allam, T. Paillard, A. Trembleau, I. Caillé

ABSTRACT

The Fragile X Syndrome (FXS) is the most common form of inherited intellectual disability, and the first monogenic cause of Autism Spectrum Disorder. FXS is caused by the absence of the RNA-binding protein FMRP (Fragile X Mental Retardation Protein).

Neuronal migration is an essential step of brain development allowing displacement of neurons from their germinal niches to their final integration site.

The role of FMRP in tangential neuronal migration remains unexplored. We studied the consequences of FMRP absence on tangential migration, using the postnatal Rostral Migratory Stream (RMS) as an experimental system.

In *Fmr1-null* RMS, neurons exhibit a slowed-down migration and an impaired trajectory, associated with defects of their centrosomal movement. Through RNA-interference-induced knock-down of *Fmr1*, we show that these migratory defects are cell-autonomous. Mutated neurons also display altered morphology as well as defects in their microtubule tyrosination distribution. Finally, we show that the FMRP mRNA target involved in these defects is MAP1B (Microtubule-Associated Protein 1B), whose knock-down rescues most migratory defects.

Our results thus unveil a new neurodevelopmental role of FMRP, as a crucial actor of postnatal tangential migration, potentially important for the understanding of FXS pathophysiology.

INTRODUCTION

The Fragile X syndrome (FXS) is the most common cause of inherited intellectual disability and a leading cause of autism spectrum disorder. FXS is due to the silencing of the gene *FMR1* and loss of the encoded protein, FMRP (Fragile X Mental Retardation Protein) (Pieretti et al., 1991). FMRP is an ubiquitous RNA-binding protein, with high level of expression in the central nervous system (Gholizadeh et al., 2015). It is a general regulator of RNA metabolism and especially of mRNA local

translation in neurons (Banerjee et al., 2018). Its cognate mRNA targets are numerous and diverse, including mRNAs encoding proteins involved in neuronal plasticity like CamKIIα (Calcium Calmodulin-dependent Kinase II) and cytoskeletal proteins like MAP1B (Microtubule-Associated Protein 1B) (Ascano et al., 2012; Brown et al., 2001; Darnell et al., 2001; Miyashiro et al., 2003). *Fmr1*-null mice are the murine model of FXS and have allowed characterization of neurodevelopmental and plasticity defects consecutive to the absence of FMRP. We previously showed the essential role of FMRP in the differentiation and learning-induced structural plasticity of adult-generated olfactory bulb interneurons (Daroles et al., 2016; Scotto-Lomassese et al., 2011).

Neuronal migration is a crucial step for the establishment of neuronal circuitry. It allows the displacement of neurons from their site of birth to their final destination of differentiation. Migration defects lead to severe brain pathologies like lissencephaly and cortical heterotopia and might be involved in psychiatric disorders (Romero et al., 2018). Moreover, migration in the human infant brain appears to be even more extended than anticipated from the rodent data (Paredes et al., 2016; Sanai et al., 2011). Moro and collaborators reported periventricular heterotopia in two FXS patients, suggesting a role for FMRP in migration (Moro et al., 2006). However, the question of potential migration defects in FXS remains mostly unexplored. In *Fmr1*-null mice, radially migrating embryonic glutamatergic cortical neurons display a defect in the multipolar to bipolar transition (La Fata et al., 2014), a critical change of polarity taking place before the initiation of the movement. Wu and collaborators additionally report a role for FMRP in regulating cortical radial migration, with its overexpression or knock-down leading to misplacement of cortical neurons (Wu et al, 2019). However, to our knowledge, tangential migration has not been studied so far and more generally the dynamics of mutated *Fmr1* neurons have never been analyzed in detail.

The Rostral Migratory Stream (RMS) is the main avenue for tangentially migrating neurons in the postnatal and adult mouse brain (Lois et al., 1996; Wichterle et al., 1997). A massive number of neuroblasts are constantly produced in the ventricular/subventricular zone (V/SVZ) and migrate over a long distance along the RMS to the olfactory bulb (OB). Like all migrating neurons, they display a cyclic saltatory mode of migration, in which the nucleus and centrosome move forward in a

“two-stroke” cycle. The centrosome moves first within a swelling in the leading process and the nucleus follows subsequently (Bellion et al., 2005).

Here, using the postnatal RMS as a migration model as in (Stoufflet et al., 2020), we show entirely novel migratory defects induced by the absence of FMRP. Migrating neurons display a slowed-down and more erratic migration in *Fmr1*-null mice, accompanied by defects in their centrosome movement. These defects are cell-autonomous, since recapitulated by RNA-interference-induced *Fmr1* knock-down (KD). Mutated neurons display morphological defects as well as altered microtubule tyrosination distribution. Given the link of MAP1B with microtubules (MTs) and its role in their tyrosination (Utreras et al., 2008), we suspected that MAP1B might be the FMRP mRNA target involved in the observed migratory defects. MAP1B level is indeed increased in the mutated RMS and its downregulation rescues most migration defects, showing that FMRP regulates neuronal migration through MAP1B translation.

MATERIAL AND METHODS

Mouse lines

Mice were housed in a 12 hours light/dark cycle, in cages containing one or two females and one male. The postnatal mice were housed in their parents’ cage. Animal care was conducted in accordance with standard ethical guidelines [National Institutes of Health (NIH) publication no. 85-23, revised 1985 and European Committee Guidelines on the Care and Use of Laboratory Animals 86/609/EEC]. The experiments were approved by the local ethics committee (Comité d’Ethique en Expérimentation Animale Charles Darwin C2EA-05 and the French Ministère de l’Education Nationale, de l’Enseignement Supérieur et de la Recherche APAFIS#13624-2018021915046521_v5). We strictly performed this approved procedure. The mice used were in a C57BL6-J background. *Fmr1-null* mice were genotyped according to the original protocol (Consorthium et al. 1994).

Plasmid constructions

pCaggs-GFP was designed in the laboratory. pCs2-centrin-RFP was ordered to Addgene (no. 26753). All the plasmids were used at concentrations between 5 to 8 mg/ml (0.01% Fast green) for postnatal injection/electroporation.

MiRNA production

Silencing of *Fmr1* and *Map1b* has been performed using BLOCK-iT Pol II miR RNAi Expression Vector Kits (Invitrogen) and the RNAi Designer (Invitrogen). The sequences of the single-stranded oligos are:
Fmr1 Top:
TGCTGTACAAATGCCTTGTAGAAAGCGTTTTGGCCAACTGACTGACGCTTTCTAAGGCATTTGTA,
Fmr1 Bottom:
CCTGTACAAATGCCTTAGAAAGCGTCAGTCAGTGGCCAAAACGCTTTCTACAAGGCATTTGTAC,
Map1b Top:
TGCTGTGTTGATGAAGTCTTGGAGATGTTTTGGCCACTGACTGACATCTCCAACTTCATCAACA,
Map1b Bottom:
CCTGTGTTGATGAAGTTGGAGATGTCAGTCAGTGGCCAAAACATCTCCAAGACTTCATCAACAC.
The double-stranded oligos were inserted in a pcDNA 6.2-GW/EmGFP-miR. The resulting constructions were sequenced before use.

Postnatal electroporation

Postnatal injection and electroporation were performed at postnatal day 2 (P2). Postnatal mice were anesthetized by hypothermia. Pseudo-stereotaxic injection [from lambda medial-lateral (M/L): 0,9; anterior-posterior (A/P): 1,1; dorsal-ventral (D/V): 2] using a glass micropipette (Drummond Scientific Company, Wiretrol I, 5-000-1050) was performed, and 2ul of plasmid (between 5 and 8 mg/ml) was injected. Animals were subjected to 5 pulses of 99.9V during 50ms separated by 950ms using the CUY21 SC Electroporator and 10-mm tweezer electrodes (Harvard Apparatus, Tweezertrode, 10mm, 45-0119). The animals were placed on 37°C plates to restore

their body temperature before returning in their parents' cage. Animals were considered as fully restored when moving naturally and their skin color returned to pink.

Postnatal acute brain slices

Brain slices of mice aged from P6 to P10 were prepared as previously described (Stoufflet et al. 2020). Pups were sacrificed by decapitation and the brain was removed from the skull. Sagittal brain sections (250 mm) were cut with a VT1200S microtome (Leica). Slices were prepared in an ice-cold cutting solution of the following composition: 125 mM NaCl, 0.4 mM $CaCl_2$, 1 mM $MgCl_2$, 1.25 mM NaH_2PO_4, 26 mM $NaHCO_3$, 5 mM sodium pyruvate, 20 mM glucose and 1 mM kynurenic acid, saturated with 5% CO_2 and 95% O_2. Slices were incubated in this solution for 30 minutes at room temperature and then placed in recording solution (identical to the cutting solution, except that the $CaCl_2$ concentration is 2 mM and kynurenic acid is absent) for at least 30 minutes at 32°C before image acquisition.

Time-lapse video microscopy of postnatal slices

To analyze neuronal migration and centrosome dynamics, images were obtained with an inverted SP5D confocal microscope (Leica) using a 40x/1.25-numerical aperture (N.A.) objective with 1.5 optical zoom or an upright SP5 MPII two-photon microscope (Leica) using a 25x/0.95-N.A. objective with 1.86 optical zoom. Images were acquired every 3 minutes for 2 to 3 hours with a 1 mm interval. The temperature in the microscope chamber was maintained at 32°C during imaging and brain slices were continuously perfused with heated recording solution (see above) saturated with 5% CO_2 and 95% O_2.

Analyses of neuronal migration and centrosome movement

Analyses were performed using ImageJ (NIH Image; National Institutes of Health, Bethesda, MD) software and MTrackJ plugin (Meijering, Dzyubachyk, et Smal 2012). The nucleus and the centrosome (when centrin-RFP was co-injected) were tracked manually on each time frame during the whole movie. We considered a NK as a

movement superior to 6 mm between two consecutive time points (3 minutes-interval). For cell migration, calculation of speed, percentage of pausing time, sinuosity, directionality, NK distance and frequency was performed using the x,y,t coordinates of the nucleus of each cell. Cells tracked less than 30 minutes and cells that didn't perform any NK during the whole tracking were excluded. A CK was defined as a forward movement superior to 2 mm followed by a backward movement superior to 2 mm. For centrosome movement, calculation of CK speed, frequency and efficiency was performed using the x,y,t coordinates of the centrosome of each cell and the x,y,t coordinates of each corresponding nucleus.

Immunohistochemistry

P7 to P10 mice were lethally anesthetized using Euthasol. Intracardiac perfusion with 4% paraformaldehyde was performed. The brain was post-fixed overnight in 4% paraformaldehyde and then rinsed three times with phosphate-buffered saline (PBS) 1x (Gibco, 1400-067). 50 mm sagittal sections were made with VT1200S microtome (Leica). Slices were placed 1 hour in a saturation solution (10% fetal bovine serum; 0.5% Triton X-100 in PBS). Primary antibodies used in this study are: GFP (Aves; GFP-1020; 1/1000), FMRP (Developmental Studies Hybridoma Bank; 1-204; 1/200), MAP1B (Santa Cruz Biotechnology; sc-365668; 1/300). The antibodies were diluted in saturation solution. Slices were incubated for 48 to 72 hours at 4°C under agitation with the antibodies and then rinsed three times with PBS 1x. Secondary antibodies used are: anti-chicken immunoglobulin Y (IgY) Alexa Fluor 488 (1/1000; Jackson ImmunoResearch; 703-545-155) against anti-GFP, anti-mouse immunoglobulin G2b (IgG2b) Alexa Fluor 555 (1/2000; Jackson ImmunoResearch; 703-545-155) against anti-FMRP and anti-MAP1B. The antibodies were diluted in saturation solution. Slices were incubated with secondary antibodies for 1 hour at room temperature under agitation, protected from light. After rinsing three times with PBS 1x, slices were counter-colored with Hoechst and mounted in Mowiol.

Tissue collection and Western blotting

RMS were manually micro-dissected from 5 to 6 postnatal mouse brains and pooled in a PBS 1x (0.5% glucose) solution. After centrifugation, protein extraction is

performed on the tissue pellet. Samples are homogenized in a lysis buffer with the following composition: 25 mM Tris HCl pH 7.5, 150 mM NaCl, 1% NP40, 0.5% NaDeoxycholate, 1 mM EDTA, 5% glycerol, 1X EDTA-free protease inhibitor cocktail (Sigma, 4693132001). After centrifugation, samples were loaded and run in NuPAGE 3-8% Tris-Acetate Gel (Invitrogen, EA0378BOX) at 120V for 15 minutes then 180V for 40 minutes. Transfer to nitrocellulose Immobilon-PVDF-P membrane (Millipore, IPVH00010) was performed at 40V overnight at 4°C. Samples are subjected to SDS/PAGE. The membrane was then saturated for 1 hour in TBSt containing 5% powder milk. Primary antibodies used are: MAP1B (Santa Cruz Biotechnology, sc-365668, 1/100), Vinculin (Cell Signaling Technology, 13901S, 1/1000). The antibodies were diluted in TBSt containing 5% powder milk. Secondary antibodies used are: ECL anti-mouse immunoglobulin G (IgG) horseradish peroxidase linked whole antibody (1/10 000; Fisher Scientific; NXA931V) against anti-MAP1B, Peroxidase-conjuguated AffiniPure F(ab')2 Fragment Donkey Anti-Rabbit IgG (H+L) minimal cross-reaction to Bovine, Chicken, Goat, Guinea Pig, Syrian Hamster, Horse, Human, Mouse, Rat, and Sheep (1/5 000; Jackson ImmunoResearch; 711-036-152) against anti-Vinculin. The antibodies were diluted in TBSt containing 5% powder milk. Labeling was visualized using Pierce ECL Western Blotting Substrate (Thermo Scientific; 32209) and luminescent image analyzer LAS-3000.

SVZ 3D-cultures and immunostaining

For miR*Map1b* efficiency quantification, brains were previously intraventricularly injected and electroporated with either miR*Map1b* or miRNeg control plasmid. For tyrosination/acetylation characterization, dissected brains weren't injected. In both cases, sub-ventricular zones from postnatal brains were dissected. SVZ explants were placed on glass-bottom culture dishes (MatTek Corporation; P35G-0-20-C) within 10 mL of 60% Matrigel (Corning; 356237). After Matrigel solidification (15 minutes at 37°C, 5% CO_2), culture media was added and the dishes were incubated for 4-5 days at 37°C, 5% CO_2. For immunostaining, SVZ cultures were fixed in 2% paraformaldehyde for 30 minutes and then rinsed three times with PBS 1x (Gibco, 1400-067). SVZ cultures were placed 1 hour in a saturation solution (10% fetal bovine serum; 0.5% Triton X-100 in PBS). Primary antibodies used in this study are: tyrosinated tubulin (Abcam; ab6160; 1/500), acetylated tubulin (Sigma-Aldrich; T7451; 1/500), MAP1B

(Santa Cruz Biotechnology; sc-365668; 1/300). The antibodies were diluted in saturation solution. Cultures were incubated for 48 hours at 4°C with the antibodies and then rinsed three times with PBS 1x. Secondary antibodies used are: anti-rat immunoglobulin G (IgG (H+L)) Alexa Fluor 647 (1/500; Jackson ImmunoResearch; 112-605-167) against anti- tyrosinated tubulin, anti-mouse immunoglobulin G2b (IgG2b) Alexa Fluor 555 (1/1000; Invitrogen; A-21147) against anti- acetylated tubulin and anti-mouse immunoglobulin G2b (IgG2b) Alexa Fluor 555 (1/1000; Invitrogen; A-21147) against anti-MAP1B. The antibodies were diluted in saturation solution. Cultures were incubated with secondary antibodies for 1 hour at room temperature, protected from light. After rinsing three times with PBS 1x, slices were counter-colored with Hoechst and mounted in Mowiol. To quantify *Map1b* KD, a cell was considered MAP1B negative when it was clearly immunonegative at high magnification (objective: 25x; zoom: 4).

Statistics

All manipulations and statistical analyses were implemented with R (4.2.1, R Foundation for Statistical Computing, Vienna, Austria). Normality in the variable distributions was assessed by the Shapiro-Wilk test. Furthermore, the Levene test was performed to probe homogeneity of variances across groups. Variables that failed the Shapiro-Wilk or the Levene test were analyzed with non-parametric statistics using the one-way Kruskal-Wallis analysis of variance on ranks followed by Nemenyi test post hoc and Mann-Whitney rank sum tests for pairwise multiple comparisons. Variables that passed the normality test were analyzed by means of one-way ANOVA followed by Tukey post hoc test for multiple comparisons or by Student's *t* test for comparing two groups. Categorical variables were compared using Pearson's c^2 test or Fisher's exact test. A *p*- value of <0.05 was used as a cutoff for statistical significance. Results are presented as the means ± SEM. The statistical tests are described in each figure legend.

For the tyrosinated/acetylated colocalization analysis, a plugin of ImageJ (JACoP) was used (Bolte and Cordelières, 2006). This plugin enables the analysis of Pearson's coefficient which provides the rate of association of two fluorochromes, with 0 for no correlation and 1 for absolute correlation.

RESULTS

FMRP is expressed in tangentially migrating neurons of the postnatal RMS

We use the postnatal RMS (Rostral Migratory Stream) as a model system to study tangential migration. In this stream, neurons are born in the ventricular-subventricular niche and follow a tangential path toward the olfactory bulb (Fig. 1.A). During their progression, neurons perform a “two-stroke” cycle. Initially, the centrosome moves forward within a swelling in the leading process (centrokinesis (CK)), which is followed by a subsequent movement of the nucleus (nucleokinesis (NK)) (Fig. 1.B). The neurons then pause and the cycle initiates again.

After an *in vivo* intraventricular electroporation of a GFP-expressing plasmid in neonate mice GFP-positive neurons can be visualized in the RMS a few days later (Fig. 1.C).

FMRP is expressed in most neurons of the Central Nervous System (CNS) (Gholizadeh et al., 2015). Accordingly, immunostaining for FMRP reveals that FMRP is strongly expressed in the RMS, where most neurons appear labeled. When observing isolated GFP-labeled neurons, FMRP labeling appears as a discrete and punctate staining visible mainly in the cytoplasm both at the rear of the neuron and in the leading process and growth cone (Fig. 1.D,E).

The absence of FMRP leads to migration defects

To investigate the involvement of FMRP in postnatal tangential migration, we used the *Fmr1-null* mouse line (Consorthium et al. 1994). Time-lapse video microscopy of GFP positive neurons in the RMS shows major migratory impairments in *Fmr1-null* neurons as compared to controls (respectively movies S.1 and S.2). The position of each fluorescent neuron was tracked at each time point, generating x, y coordinates along its trajectory, thus enabling the quantification of various migration parameters. *Fmr1-null* neurons display a slowed-down migration, an increased pausing time, a more sinuous trajectory, and a lack of directionality (Fig. 2.A-D). The nucleokinesis is less frequent in *Fmr1-null* neurons and the mean distance per NK is reduced (Fig. 2.E,F). The absence of FMRP thus leads to severe migratory defects in the RMS.

The absence of FMRP impairs centrosomal dynamics

Given the central role of the centrosome in neuronal migration (Higginbotham and Gleeson, 2007), we analyzed its dynamics. We thus performed a co-electroporation of GFP and Centrine-RFP in *Fmr1-null* and control neonate mice to label migrating neurons and their centrosomes (Fig. 3.A). A simultaneous tracking of the cell body and the centrosome enabled the quantification of centrosomal dynamics. The CK is slowed-down and less frequent in *Fmr1-null* neurons, as compared to control neurons (Fig. 3.B,C). To analyze the coordination of the centrosomal and the subsequent nuclear movement, we established a parameter quantifying CK efficiency. A CK leading to a subsequent NK was defined as an efficient CK as opposed to a CK not leading to an NK. CK efficiency is reduced in *Fmr1-null* neurons as compared to control neurons (Fig. 3.D), showing that the "two-stroke" cycle is compromised. Taken together, these results show that FMRP plays a key role in RMS migration.

Fmr1 knock-down recapitulates migration defects of _Fmr1-null_ neurons

To assess whether these migration defects are cell autonomous, we designed an interfering RNA coupled to GFP to cell-autonomously knock-down *Fmr1* mRNA in RMS neurons, similar to (Scotto-Lomassese et al., 2011). The miR*Fmr1*-GFP was co-injected with centrin-RFP in C57Bl6 neonate mice and time lapse imaging was performed in acute sections of the RMS (movie S. 3). MiR*Fmr1*-GFP neurons migrate slowly, spend more time in pause, have a more sinuous and deviated trajectory as compared to neurons expressing the miRNeg control plasmid (Fig. 4.A-D). MiR*Fmr1*-GFP neurons also exhibit NK defects (Fig. 4.E,F) and CK defects (Fig. 5.A-C). Moreover, overall statistical comparisons of GFP positive *Fmr1-null* neurons and miR*Fmr1*-GFP positive neurons show no significant differences for all migratory parameters. *Fmr1* KD is thus sufficient to recapitulate the entire migratory phenotype described in *Fmr1-null* neurons, showing that FMRP cell-autonomously regulates neuronal migration.

Alterations of the morphology and of the the subcellular distribution of tyrosinated MTs in _Fmr1-null_ neurons

Because the cytoskeleton is essential to neuronal migration (Marín et al., 2010; Reiner and Sapir, 2009; Sakakibara et al., 2013; Tsai and Gleeson, 2005), we analyzed the morphology of RMS neurons in *Fmr1-null* mice. The number of processes in GFP-labeled RMS neurons was counted, showing that the proportion of cells with multiple processes is increased in *Fmr1-null* neurons compared to control neurons (Fig. 6.A,B). Moreover, the length of the leading process is decreased in *Fmr1-null* neurons compared to the control neurons (Fig. 6.C). Altogether, these results show that *Fmr1-null* neurons exhibit morphological alterations, which could be attributed to cytoskeletal defects.

Since we report morphological defects of *Fmr1-null* neurons, we investigated the subcellular distribution of two functional microtubule pools within migrating neurons. Tyrosination and acetylation are post-translational modifications of alpha-tubulin associated with respectively dynamic and stable MTs sub-networks (Moutin et al., 2021). Fixed *Fmr1-null* and control SVZs explants were stained with anti-tyrosinated and anti-acetylated tubulin (Fig. 6.D). Pearson's coefficient, which measures the relative overlap of the two tubulin subpopulations, is increased in *Fmr1-null* neurons compared to control (Fig. 6.E). These data suggest that tyrosinated and acetylated tubulins are significantly more colocalized in *Fmr1-null* neurons than in controls. This differential distribution might be associated with an alteration of MTs dynamics.

MAP1B expression is increased in *Fmr1-null* RMS neurons

MAP1B is a microtubule-associated protein expressed at early stages of brain development. MAP1B has essential roles in neuritogenesis and synaptogenesis, allowed by its ability to modulate microtubule and actin dynamics (Gonzalez-Billault et al. 2004), in particular microtubule tyrosination (Utreras et al., 2008). MAP1B mRNA is among the well-known targets of FMRP (Brown et al. 2001; Darnell et al. 2001; Zalfa et al. 2003; Zhang et al. 2001). As FMRP is a repressor of MAP1B mRNA translation, the overall level of MAP1B appears increased in an *Fmr1-null* context (Zhang et al. 2001; Lu et al. 2004).

Since *Fmr1-null* neurons exhibit migration defects associated with morphological impairments and microtubule tyrosination alteration, MAP1B appeared as an

interesting FMRP mRNA target to investigate. As described for other regions and systems (Zhang et al. 2001; Lu et al. 2004), immunostaining for MAP1B in *Fmr1-null* RMS indeed showed its overexpression (Fig. S.1.A). Quantification of MAP1B expression by western blot of the RMS confirmed that MAP1B expression is increased in *Fmr1-null* RMS as compared to controls (Fig. S.1.B).

Map1b **knock-down rescues the migratory phenotype of** ***Fmr1-null*** **neurons**

To assess whether the upregulation of MAP1B is responsible for the migratory phenotype observed in *Fmr1-null* neurons, we designed an interfering RNA, which expression was coupled to that of GFP, to cell-autonomously knock-down *Map1b* mRNA in RMS neurons. The miR*Map1b*-GFP, whose efficiency was assessed (Fig. S.2), was injected in *Fmr1-null* neonate mice and time lapse imaging was performed in acute sections of the RMS (movie S. 4). *Fmr1-null* neurons expressing miR*Map1b*-GFP exhibit a completely restored migration speed, pausing time, NK distance and frequency, which become comparable to miRNeg-GFP control neurons (Fig.7.A,B,D,E). Nonetheless, *Fmr1-null* neurons expressing miR*Map1b*-GFP still present an increased sinuosity, similar to *Fmr1-null* neurons expressing the control miRNeg-GFP plasmid (Fig.7.C). These results show that MAP1B is the main FMRP mRNA target involved in the regulation of the saltatory migration *per se* but that other FMRP targets might regulate the directionality of migrating neurons.

DISCUSSION

FMRP is commonly described as a critical regulator of neuronal plasticity and neural development (Richter and Zhao, 2021). However, its role in neuronal migration remains poorly understood. We provide here clear evidence for its cell-autonomous role in postnatal tangential migration and the causal role of its mRNA target MAP1B.

A role for FMRP in radial embryonic migration was evidenced by (La Fata et al., 2014; Wu et al., 2019). (La Fata et al., 2014) mainly analyzed defects in the multipolar to bipolar transition, which can be interpreted as a polarity defect rather than a migration defect *per se*. (Wu et al., 2019) reported neuronal misplacements after FMRP loss or gain of function in relation with Micro-RNA 129 but did not analyze the dynamic of radial migration itself. To our knowledge, tangential migration in the absence of FMRP has never been analyzed so far, and neither has been the effect of its absence on the dynamic of saltatory migration, as analyzed by live-imaging.

We report strong defects in postnatal migration with a slowed-down and erratic migration. Of importance, even though the mutated neurons are delayed in their movement and lose time finding the proper direction, they ultimately properly arrive in the OB, which we previously showed in (Scotto-Lomassese et al., 2011). Live imaging allowed us to perform detailed analysis of both nucleokinesis and centrosome dynamics, which proved both to be deeply perturbed. As microtubules are essential regulators of both processes (Kuijpers and Hoogenraad, 2011; Tsai and Gleeson, 2005) and as mutated neurons display altered morphology as well as altered pattern of microtubule tyrosination, this led us to suspect MAP1B as the key FMRP mRNA target involved in the migratory phenotypes. MAP1B is one of the historic targets of FMRP (Brown et al., 2001; Darnell et al., 2001; Zalfa et al., 2003; Zhang et al., 2001). It is expressed early in the embryonic brain (Tucker et al., 1989, 1988) and is essential to different steps of neural development (Gonzalez-Billault et al., 2004) including migration (Takei et al., 2000). It is also linked to microtubule tyrosination (Tortosa et al., 2013; Tymanskyj et al., 2012; Utreras et al., 2008).

We show MAP1B overexpression in *Fmr1*-mutated neurons and rescue the migratory defects through its RNA-interference-induced KD. This identifies MAP1B as the critical FMRP mRNA target involved in the regulation of the cyclic saltatory migration, probably through its link with microtubule tyrosination.

Of importance, the sinuosity of migrating neurons was not rescued by *Map1b* KD, suggesting that other FMRP mRNA targets might be involved in that process. FMRP has been associated with numerous targets of the actin-myosin pathway (Michaelsen-Preusse et al., 2016; Michaelsen- Preusse et al., 2018). As a consequence, one could imagine that some of them and particularly those involved in the movement of the growth cone might be involved in this process, e.g. myosin light chain kinase, Rac1, cofilin, profilin or Arp2/3 (Michaelsen- Preusse et al., 2018). Another example could be APC (Adenomatous Polyposis Coli) a recently described FMRP mRNA target (Maurin et al., 2018), involved in the regulation of both microtubules and the actin cytoskeleton in the growth cone (Koester et al., 2007).

In the context of FXS, looking at tangential migration in the probably soon to be developed FXS assembloïds (Levy and Paşca, 2022) will be of course of major interest. It is to be noted that postnatal tangential migration in the infant human brain was recently described to be even more extensive than in mice (Paredes et al., 2016; Sanai et al., 2011) so that, if conserved in humans, the defects that we observe might be critical for the postnatal corticogenesis of FXS patients.

As a conclusion, we report here an entirely new function of FMRP as a regulator of tangential migration linked to microtubules *via* MAP1B. This is important for the fundamental understanding of this multifaceted protein and might also be important for the pathophysiological understanding of FXS.

FUNDINGS

This work was funded by Fondation Jérôme Lejeune, ANR NotifX ANR-20-CE16-0016 and NIH contract NIDCD Grant R01-DC-017989.

ACKNOWLEDGMENTS

We thank Isabelle Dusart for expert reading as well as Caroline Dubacq and Oriane Trouillard for technical help. The experiments were performed in IBPS imaging facility and the mice were housed in IBPS animal facility.

REFERENCES

Ascano, M., Mukherjee, N., Bandaru, P., Miller, J.B., Nusbaum, J.D., Corcoran, D.L., Langlois, C., Munschauer, M., Dewell, S., Hafner, M., Williams, Z., Ohler, U., Tuschl, T., 2012. FMRP targets distinct mRNA sequence elements to regulate protein expression. Nature 492, 382–386. https://doi.org/10.1038/nature11737

Banerjee, A., Ifrim, M.F., Valdez, A.N., Raj, N., Bassell, G.J., 2018. Aberrant RNA translation in fragile X syndrome: From FMRP mechanisms to emerging therapeutic strategies. Brain Res. 1693, 24–36. https://doi.org/10.1016/j.brainres.2018.04.008

Bellion, A., Baudoin, J.-P., Alvarez, C., Bornens, M., Métin, C., 2005. Nucleokinesis in Tangentially Migrating Neurons Comprises Two Alternating Phases: Forward Migration of the Golgi/Centrosome Associated with Centrosome Splitting and Myosin Contraction at the Rear. J. Neurosci. 25, 5691–5699. https://doi.org/10.1523/JNEUROSCI.1030-05.2005

Bolte, S., Cordelières, F.P., 2006. A guided tour into subcellular colocalization analysis in light microscopy. J. Microsc. 224, 213–232. https://doi.org/10.1111/j.1365-2818.2006.01706.x

Brown, V., Jin, P., Ceman, S., Darnell, J.C., O'Donnell, W.T., Tenenbaum, S.A., Jin, X., Feng, Y., Wilkinson, K.D., Keene, J.D., Darnell, R.B., Warren, S.T., 2001. Microarray identification of FMRP-associated brain mRNAs and altered mRNA translational profiles in fragile X syndrome. Cell 107, 477–487. https://doi.org/10.1016/s0092-8674(01)00568-2

Bülow, P., Segal, M., Bassell, G.J., 2022. Mechanisms Driving the Emergence of Neuronal Hyperexcitability in Fragile X Syndrome. Int. J. Mol. Sci. 23, 6315. https://doi.org/10.3390/ijms23116315

Consorthium, The Dutch-Belgian Fragile X., Cathy E. Bakker, Coleta Verheij, Rob Willemsen, Robert van der Helm, Frank Oerlemans, Marcel Vermey, et al. 1994. « Fmr1 Knockout Mice: A Model to Study Fragile X Mental Retardation ». *Cell* 78 (1): 23- 33. https://doi.org/10.1016/0092-8674(94)90569-X.

Darnell, J. C., K. B. Jensen, P. Jin, V. Brown, S. T. Warren, et R. B. Darnell. 2001. « Fragile X Mental Retardation Protein Targets G Quartet MRNAs Important for Neuronal Function ». *Cell* 107 (4): 489- 99. https://doi.org/10.1016/s0092-8674(01)00566-9.

Daroles, L., Gribaudo, S., Doulazmi, M., Scotto-Lomassese, S., Dubacq, C., Mandairon, N., Greer, C.A., Didier, A., Trembleau, A., Caillé, I., 2016. Fragile X Mental Retardation Protein and Dendritic Local Translation of the Alpha Subunit of the Calcium/Calmodulin-Dependent Kinase II Messenger RNA Are Required for the Structural Plasticity Underlying Olfactory Learning. Biol. Psychiatry 80, 149–159. https://doi.org/10.1016/j.biopsych.2015.07.023

Gholizadeh, S., Halder, S.K., Hampson, D.R., 2015. Expression of fragile X mental retardation protein in neurons and glia of the developing and adult mouse brain. Brain Res. 1596, 22–30. https://doi.org/10.1016/j.brainres.2014.11.023

Gonzalez-Billault, C., Avila, J., Cáceres, A., 2001. Evidence for the role of MAP1B in axon formation. Mol. Biol. Cell 12, 2087–2098. https://doi.org/10.1091/mbc.12.7.2087

Gonzalez-Billault, C., Jimenez-Mateos, E.M., Caceres, A., Diaz-Nido, J., Wandosell, F., Avila, J., 2004. Microtubule-associated protein 1B function during normal development, regeneration, and pathological conditions in the nervous system. J. Neurobiol. 58, 48–59. https://doi.org/10.1002/neu.10283

Higginbotham, H.R., Gleeson, J.G., 2007. The centrosome in neuronal development. Trends Neurosci. 30, 276–283. https://doi.org/10.1016/j.tins.2007.04.001

Koester, M.P., Müller, O., Pollerberg, G.E., 2007. Adenomatous polyposis coli is differentially distributed in growth cones and modulates their steering. J. Neurosci. Off. J. Soc. Neurosci. 27, 12590–12600. https://doi.org/10.1523/JNEUROSCI.2250-07.2007

Kuijpers, M., Hoogenraad, C.C., 2011. Centrosomes, microtubules and neuronal development. Mol. Cell. Neurosci. 48, 349–358. https://doi.org/10.1016/j.mcn.2011.05.004

La Fata, G., Gärtner, A., Domínguez-Iturza, N., Dresselaers, T., Dawitz, J., Poorthuis, R.B., Averna, M., Himmelreich, U., Meredith, R.M., Achsel, T., Dotti, C.G., Bagni, C.,

2014. FMRP regulates multipolar to bipolar transition affecting neuronal migration and cortical circuitry. Nat. Neurosci. 17, 1693–1700. https://doi.org/10.1038/nn.3870

Lee, F.H.F., Lai, T.K.Y., Su, P., Liu, F., 2019. Altered cortical Cytoarchitecture in the Fmr1 knockout mouse. Mol. Brain 12, 56. https://doi.org/10.1186/s13041-019-0478-8

Levy, R.J., Paşca, S.P., 2022. What Have Organoids and Assembloids Taught Us About the Pathophysiology of Neuropsychiatric Disorders? Biol. Psychiatry S0006-3223(22)01797–8. https://doi.org/10.1016/j.biopsych.2022.11.017

Lois, C., García-Verdugo, J.M., Alvarez-Buylla, A., 1996. Chain migration of neuronal precursors. Science 271, 978–981. https://doi.org/10.1126/science.271.5251.978

Lu, Robert, Houping Wang, Zhe Liang, Li Ku, William T. O'donnell, Wen Li, Stephen T. Warren, et Yue Feng. 2004. « The Fragile X Protein Controls Microtubule-Associated Protein 1B Translation and Microtubule Stability in Brain Neuron Development ». *Proceedings of the National Academy of Sciences of the United States of America* 101 (42): 15201- 6. https://doi.org/10.1073/pnas.0404995101.

Marín, O., Valiente, M., Ge, X., Tsai, L.-H., 2010. Guiding Neuronal Cell Migrations. Cold Spring Harb. Perspect. Biol. 2, a001834. https://doi.org/10.1101/cshperspect.a001834

Maurin, T., Lebrigand, K., Castagnola, S., Paquet, A., Jarjat, M., Popa, A., Grossi, M., Rage, F., Bardoni, B., 2018. HITS-CLIP in various brain areas reveals new targets and new modalities of RNA binding by fragile X mental retardation protein. Nucleic Acids Res. 46, 6344–6355. https://doi.org/10.1093/nar/gky267

Meijering, Erik, Oleh Dzyubachyk, et Ihor Smal. 2012. « Methods for Cell and Particle Tracking ». *Methods in Enzymology* 504: 183- 200. https://doi.org/10.1016/B978-0-12-391857-4.00009-4.

Michaelsen-Preusse, K., Zessin, S., Grigoryan, G., Scharkowski, F., Feuge, J., Remus, A., Korte, M., 2016. Neuronal profilins in health and disease: Relevance for spine plasticity and Fragile X syndrome. Proc. Natl. Acad. Sci. U. S. A. 113, 3365–3370. https://doi.org/10.1073/pnas.1516697113

Michaelsen- Preusse, K., Feuge, J., Korte, M., 2018. Imbalance of synaptic actin dynamics as a key to fragile X syndrome? J. Physiol. 596, 2773–2782. https://doi.org/10.1113/JP275571

Miyashiro, K.Y., Beckel-Mitchener, A., Purk, T.P., Becker, K.G., Barret, T., Liu, L., Carbonetto, S., Weiler, I.J., Greenough, W.T., Eberwine, J., 2003. RNA cargoes associating with FMRP reveal deficits in cellular functioning in Fmr1 null mice. Neuron 37, 417–431. https://doi.org/10.1016/s0896-6273(03)00034-5

Moro, F., Pisano, T., Bernardina, B.D., Polli, R., Murgia, A., Zoccante, L., Darra, F., Battaglia, A., Pramparo, T., Zuffardi, O., Guerrini, R., 2006. Periventricular heterotopia in fragile X syndrome. Neurology 67, 713–715. https://doi.org/10.1212/01.wnl.0000230223.51595.99

Moutin, M.-J., Bosc, C., Peris, L., Andrieux, A., 2021. Tubulin post-translational modifications control neuronal development and functions. Dev. Neurobiol. 81, 253–272. https://doi.org/10.1002/dneu.22774

Paredes, M.F., James, D., Gil-Perotin, S., Kim, H., Cotter, J.A., Ng, C., Sandoval, K., Rowitch, D.H., Xu, D., McQuillen, P.S., Garcia-Verdugo4, J.-M., Huang, E.J., Alvarez-Buylla, A., 2016. Extensive migration of young neurons into the infant human frontal lobe. Science 354. https://doi.org/10.1126/science.aaf7073

Pieretti, M., Zhang, F.P., Fu, Y.H., Warren, S.T., Oostra, B.A., Caskey, C.T., Nelson, D.L., 1991. Absence of expression of the FMR-1 gene in fragile X syndrome. Cell 66, 817–822. https://doi.org/10.1016/0092-8674(91)90125-i

Reiner, O., Sapir, T., 2009. Polarity regulation in migrating neurons in the cortex. Mol. Neurobiol. 40, 1–14. https://doi.org/10.1007/s12035-009-8065-0

Richter, J.D., Zhao, X., 2021. The Molecular Biology of FMRP: New Insights into Fragile X Syndrome. Nat. Rev. Neurosci. 22, 209–222. https://doi.org/10.1038/s41583-021-00432-0

Romero, D.M., Bahi-Buisson, N., Francis, F., 2018. Genetics and mechanisms leading to human cortical malformations. Semin. Cell Dev. Biol. 76, 33–75. https://doi.org/10.1016/j.semcdb.2017.09.031

Sakakibara, A., Ando, R., Sapir, T., Tanaka, T., 2013. Microtubule dynamics in neuronal morphogenesis. Open Biol. 3, 130061. https://doi.org/10.1098/rsob.130061

Sanai, N., Nguyen, T., Ihrie, R.A., Mirzadeh, Z., Tsai, H.-H., Wong, M., Gupta, N., Berger, M.S., Huang, E., Garcia-Verdugo, J.-M., Rowitch, D.H., Alvarez-Buylla, A., 2011. Corridors of migrating neurons in the human brain and their decline during infancy. Nature 478, 382–386. https://doi.org/10.1038/nature10487

Scotto-Lomassese, S., Nissant, A., Mota, T., Néant-Féry, M., Oostra, B.A., Greer, C.A., Lledo, P.-M., Trembleau, A., Caillé, I., 2011. Fragile X mental retardation protein regulates new neuron differentiation in the adult olfactory bulb. J. Neurosci. Off. J. Soc. Neurosci. 31, 2205–2215. https://doi.org/10.1523/JNEUROSCI.5514-10.2011

Stoufflet, Julie, Maxime Chaulet, Mohamed Doulazmi, Coralie Fouquet, Caroline Dubacq, Christine Métin, Sylvie Schneider-Maunoury, Alain Trembleau, Pierre Vincent, et Isabelle Caillé. 2020. « Primary Cilium-Dependent CAMP/PKA Signaling at the Centrosome Regulates Neuronal Migration ». *Science Advances* 6 (36): eaba3992. https://doi.org/10.1126/sciadv.aba3992.

Takei, Y., Teng, J., Harada, A., Hirokawa, N., 2000. Defects in axonal elongation and neuronal migration in mice with disrupted tau and map1b genes. J. Cell Biol. 150, 989–1000. https://doi.org/10.1083/jcb.150.5.989

Tortosa, E., Galjart, N., Avila, J., Sayas, C.L., 2013. MAP1B regulates microtubule dynamics by sequestering EB1/3 in the cytosol of developing neuronal cells. EMBO J. 32, 1293–1306. https://doi.org/10.1038/emboj.2013.76

Tsai, L.-H., Gleeson, J.G., 2005. Nucleokinesis in neuronal migration. Neuron 46, 383–388. https://doi.org/10.1016/j.neuron.2005.04.013

Tucker, R.P., Binder, L.I., Matus, A.I., 1988. Neuronal microtubule-associated proteins in the embryonic avian spinal cord. J. Comp. Neurol. 271, 44–55. https://doi.org/10.1002/cne.902710106

Tucker, R.P., Garner, C.C., Matus, A., 1989. In situ localization of microtubule-associated protein mRNA in the developing and adult rat brain. Neuron 2, 1245–1256. https://doi.org/10.1016/0896-6273(89)90309-7

Tymanskyj, S.R., Scales, T.M.E., Gordon-Weeks, P.R., 2012. MAP1B enhances microtubule assembly rates and axon extension rates in developing neurons. Mol. Cell. Neurosci. 49, 110–119. https://doi.org/10.1016/j.mcn.2011.10.003

Utreras, E., Jiménez-Mateos, E.M., Contreras-Vallejos, E., Tortosa, E., Pérez, M., Rojas, S., Saragoni, L., Maccioni, R.B., Avila, J., González-Billault, C., 2008. Microtubule-associated protein 1B interaction with tubulin tyrosine ligase contributes to the control of microtubule tyrosination. Dev. Neurosci. 30, 200–210. https://doi.org/10.1159/000109863

Wichterle, H., García-Verdugo, J.M., Alvarez-Buylla, A., 1997. Direct Evidence for Homotypic, Glia-Independent Neuronal Migration. Neuron 18, 779–791. https://doi.org/10.1016/S0896-6273(00)80317-7

Wu, C., Zhang, X., Chen, P., Ruan, X., Liu, W., Li, Y., Sun, C., Hou, L., Yin, B., Qiang, B., Shu, P., Peng, X., 2019. MicroRNA-129 modulates neuronal migration by targeting Fmr1 in the developing mouse cortex. Cell Death Dis. 10, 287. https://doi.org/10.1038/s41419-019-1517-1

Zalfa, Francesca, Marcello Giorgi, Beatrice Primerano, Annamaria Moro, Alessandra Di Penta, Surya Reis, Ben Oostra, et Claudia Bagni. 2003. « The Fragile X Syndrome Protein FMRP Associates with BC1 RNA and Regulates the Translation of Specific MRNAs at Synapses ». *Cell* 112 (3): 317- 27. https://doi.org/10.1016/s0092-8674(03)00079-5.

Zhang, Y. Q., A. M. Bailey, H. J. Matthies, R. B. Renden, M. A. Smith, S. D. Speese, G. M. Rubin, et K. Broadie. 2001. « Drosophila Fragile X-Related Gene Regulates the MAP1B Homolog Futsch to Control Synaptic Structure and Function ». *Cell* 107 (5): 591- 603. https://doi.org/10.1016/s0092-8674(01)00589-x.

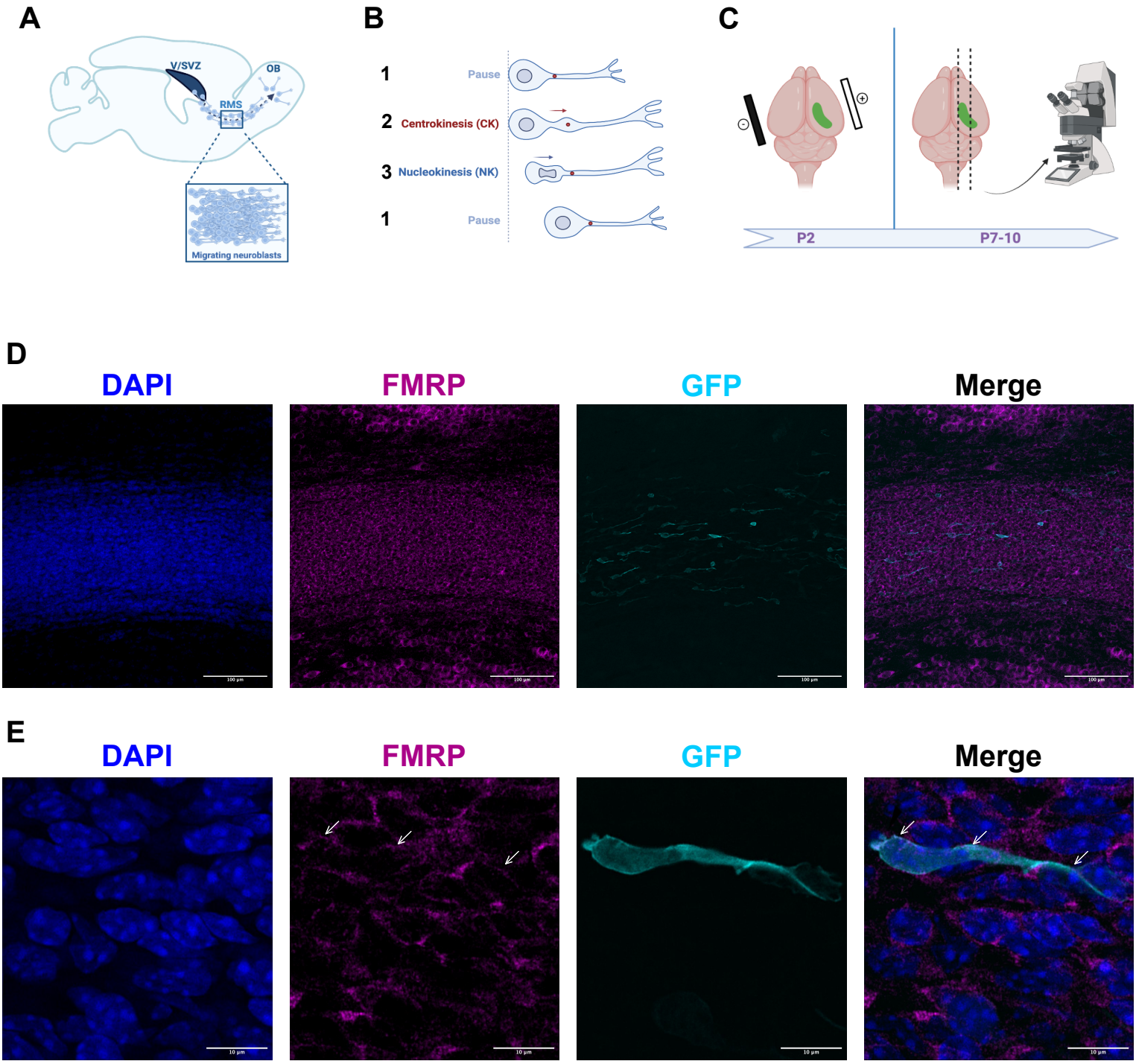

FIGURE 1. ***FMRP is expressed in migrating neurons of the murine postnatal RMS.*** *(A) Scheme of a sagittal section of the postnatal RMS connecting the V/SVZ to the OB. V/SVZ, ventricular/sub-ventricular zone; OB, olfactory bulb; RMS, rostral migratory stream. The inset shows the high density of homotypically migrating neurons in the RMS. (B) Representation of neuroblasts' cyclic saltatory migration. 1. The neuron is in pause. 2. The leading process (LP) extends, and the centrosome moves within a swelling in the LP. 3. The nucleus moves forward. CK, centrokinesis; NK, nucleokinesis. (C) Scheme of the experimental procedure. 2-day old neonates are intraventricularly electroporated with a GFP-expressing plasmid to label a cohort of migrating neurons that can be subsequently visualized in fixed or acute sections of the RMS. (D) Immunohistochemistry of the RMS showing FMRP expression (magenta) along the stream, in which a cohort of GFP-positive neurons (cyan) are visible. Scale bar: 100 µm. (E) Immunohistochemistry of a GFP-positive RMS neuron (cyan) showing FMRP subcellular expression (magenta). The GFP-positive neuron displays a cytoplasmic expression of FMRP around the nucleus (indicated by white arrows), along the leading process and in the growth cone. The surrounding GFP-negative neurons express FMRP as well, according to the same pattern. Scale bar: 10 µm.*

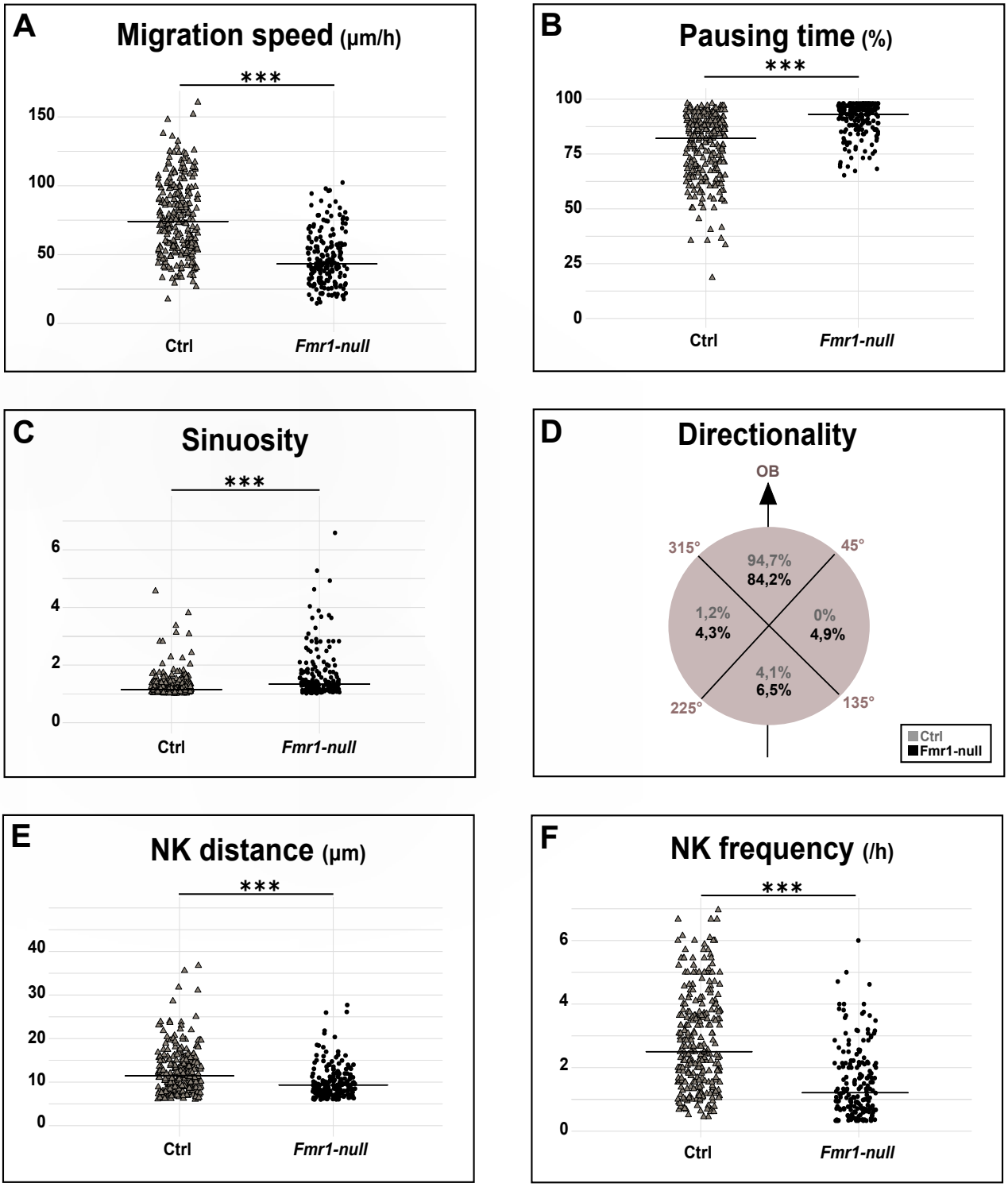

FIGURE 2. ***Migration defects in Fmr1-null neurons.*** *(A) Migration speed of control (Ctrl) and Fmr1-null neurons. Ctrl: 76 ± 2 µm/h; Fmr1-null: 47 ± 1 µm/h (Mann-Whitney test, p-value < 0.001). (B) Percentage of pausing time of control and Fmr1-null neurons. Ctrl: 78 %; Fmr1-null: 91 % (Mann-Whitney test, p-value < 0.001). (C) Sinuosity index of control and Fmr1-null neurons. Ctrl: 1.32 ± 0.04; Fmr1-null: 1.93 ± 0.16 (Mann-Whitney test, p-value < 0.001). (D) Migration directionality radar represented in four spatial dials. Percentage of cells migrating in each spatial direction in control and Fmr1-null neurons, relatively to the vector going straight from the SVZ to the OB. (Fisher's Exact test, p-value < 0.001). (E) NK mean distance of control and Fmr1-null neurons. Ctrl: 12.5 ± 0.3 µm; Fmr1-null: 10.9 ± 0.8 µm (Mann-Whitney test, p-value < 0.001). (F) NK frequency of control and Fmr1-null neurons. Ctrl: 2.9 ± 0.1 NK/h; Fmr1-null: 1.5 ± 0.1 NK/h (Mann-Whitney test, p-value < 0.001). The black line represents the median. Ctrl: N = 3, n = 275; Fmr1-null: N = 3, n = 184. ***p-value < 0.001.*

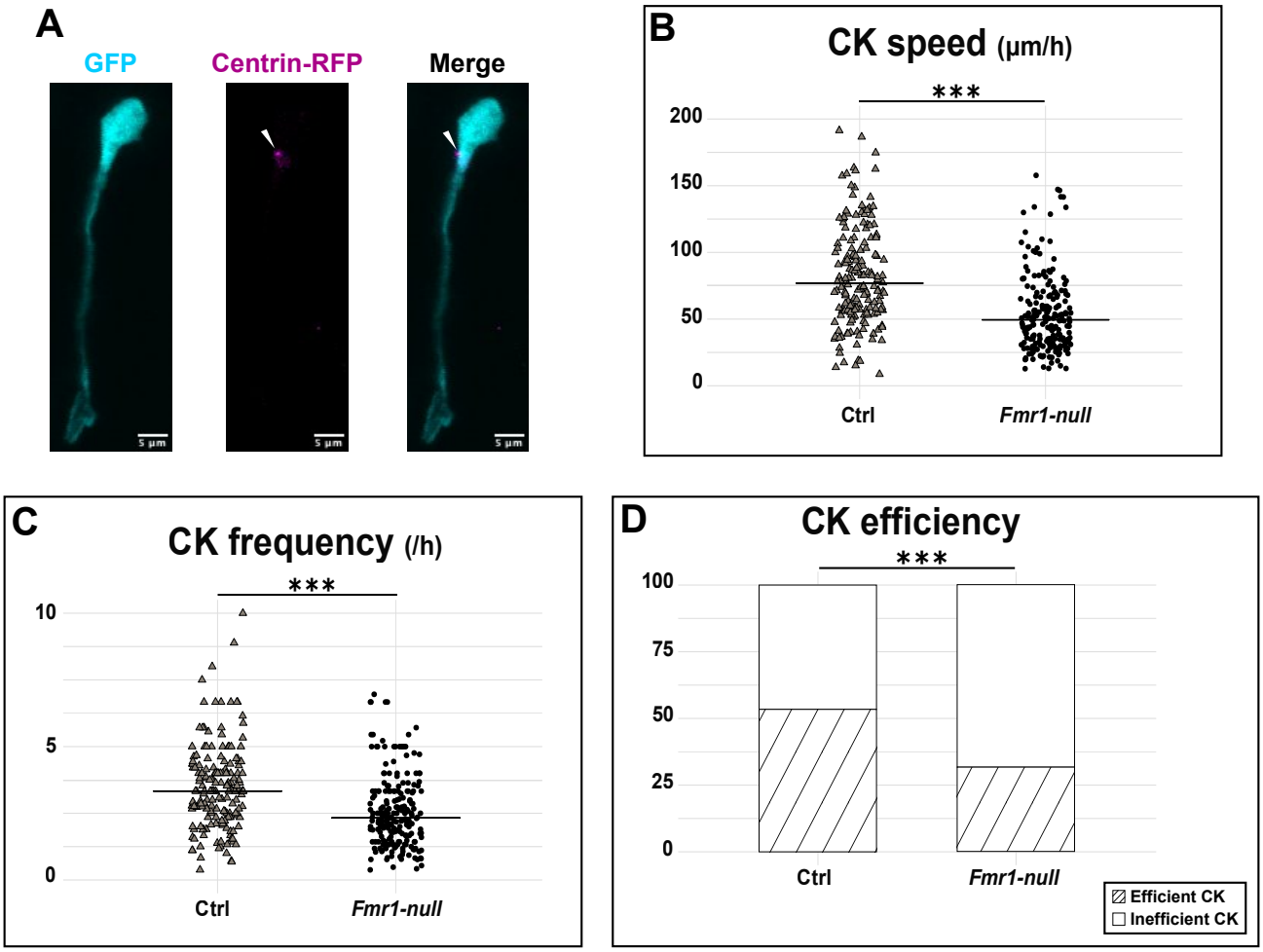

FIGURE 3. *CK defects in Fmr1-null neurons.* *(A) Illustration of an RMS-migrating neuron (cyan) co-injected with centrin-RFP (magenta). Scale bar: 5 µm. (B) CK speed of control and Fmr1-null neurons. Ctrl: 82 ± 3 µm/h; Fmr1-null: 54 ± 2 µm/h (Mann-Whitney test, p-value < 0.001). (C) CK frequency of control and Fmr1-null neurons. Ctrl: 3.5 ± 0.1 CK/h; Fmr1-null: 2.6 ± 0.1 CK/h (Mann-Whitney test, p-value < 0.001). (D) Percentage of efficient CKs in control and Fmr1-null neurons. Ctrl: 54 %; Fmr1-null: 33 % (Chi2 = 57.611, p-value < 0.001). The black line represents the median. Ctrl: N = 3, n = 178; Fmr1-null: N = 3, n = 216. *** p-value < 0.001.*

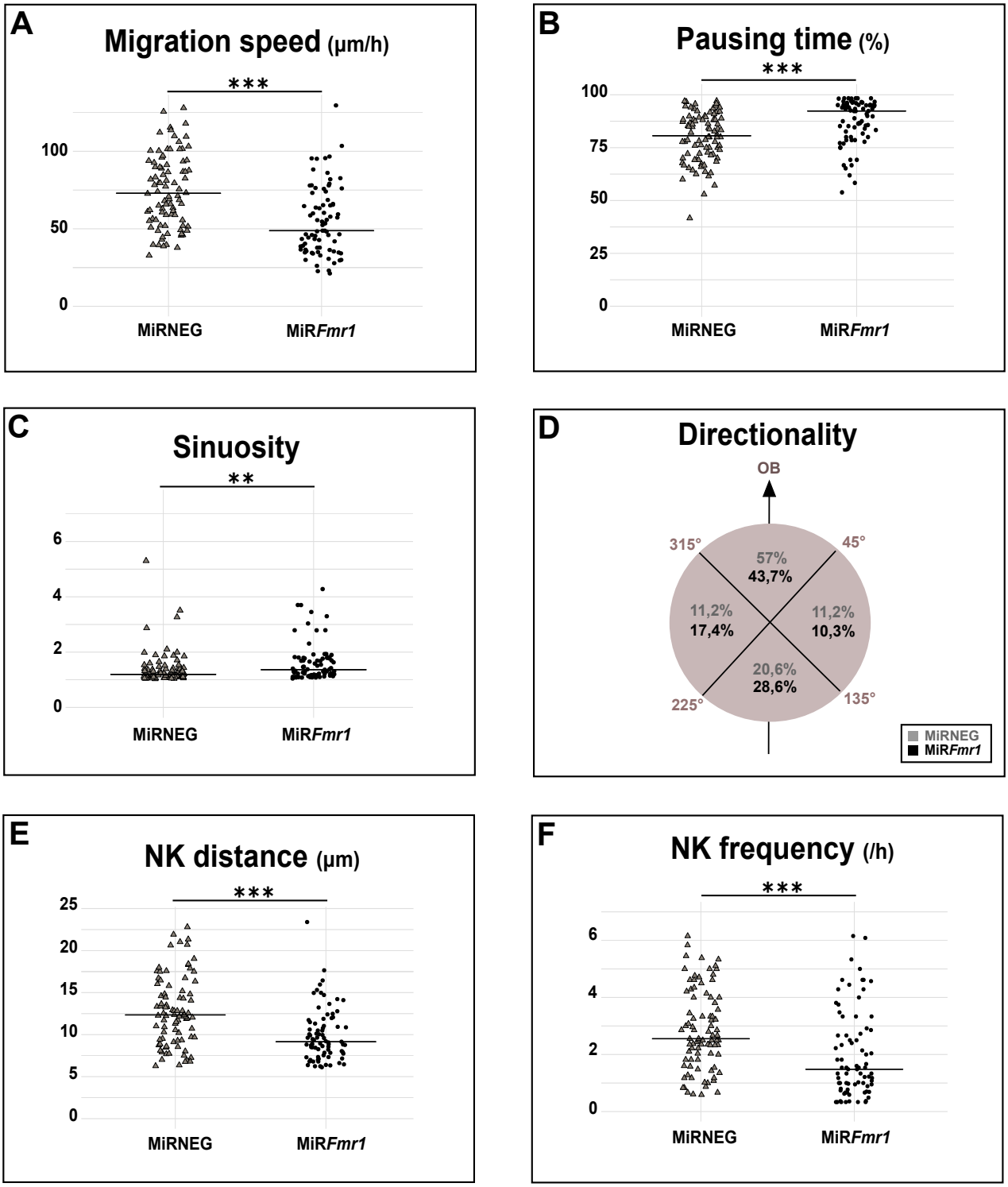

FIGURE 4. *Fmr1 KD recapitulates Fmr1-null neuronal migration defects.* *(A) Migration speed of neurons expressing MiRNEG and MiRFmr1. MiRNEG: 75 ± 3 µm/h; MiRFmr1: 55 ± 2 µm/h (Mann-Whitney test, p-value < 0.001). (B) Percentage of pausing time of neurons expressing MiRNEG and MiRFmr1. MiRNEG: 80 %; MiRFmr1: 88 % (Mann-Whitney test, p-value < 0.001). (C) Sinuosity index of neurons expressing MiRNEG and MiRFmr1. MiRNEG: 1.50 ± 0.12; MiRFmr1: 1.62 ± 0.08 (Mann-Whitney test, p-value = 0.003). (D) Migration directionality radar represented in four spatial dials. Percentage of cells migrating in each spatial direction in neurons expressing MiRNEG and MiRFmr1, relatively to the vector going straight from the SVZ to the OB. (Fisher's Exact test, p-value = 0.019). (E) NK mean distance of neurons expressing MiRNEG and MiRFmr1. MiRNEG: 12.8 ± 0.4 µm; MiRFmr1: 9.9 ± 0.4 µm (Mann-Whitney test, p-value < 0.001). (F) NK frequency of neurons expressing MiRNEG and MiRFmr1. MiRNEG: 2.9 ± 0.2 NK/h; MiRFmr1: 2.0 ± 0.2 NK/h (Mann-Whitney test, p-value < 0.001). The black line represents the median. MiRNEG: N = 3, n = 86; MiRFmr1: N = 3, n = 79. * p-value < 0.05; ** p-value < 0.005; *** p-value < 0.001.*

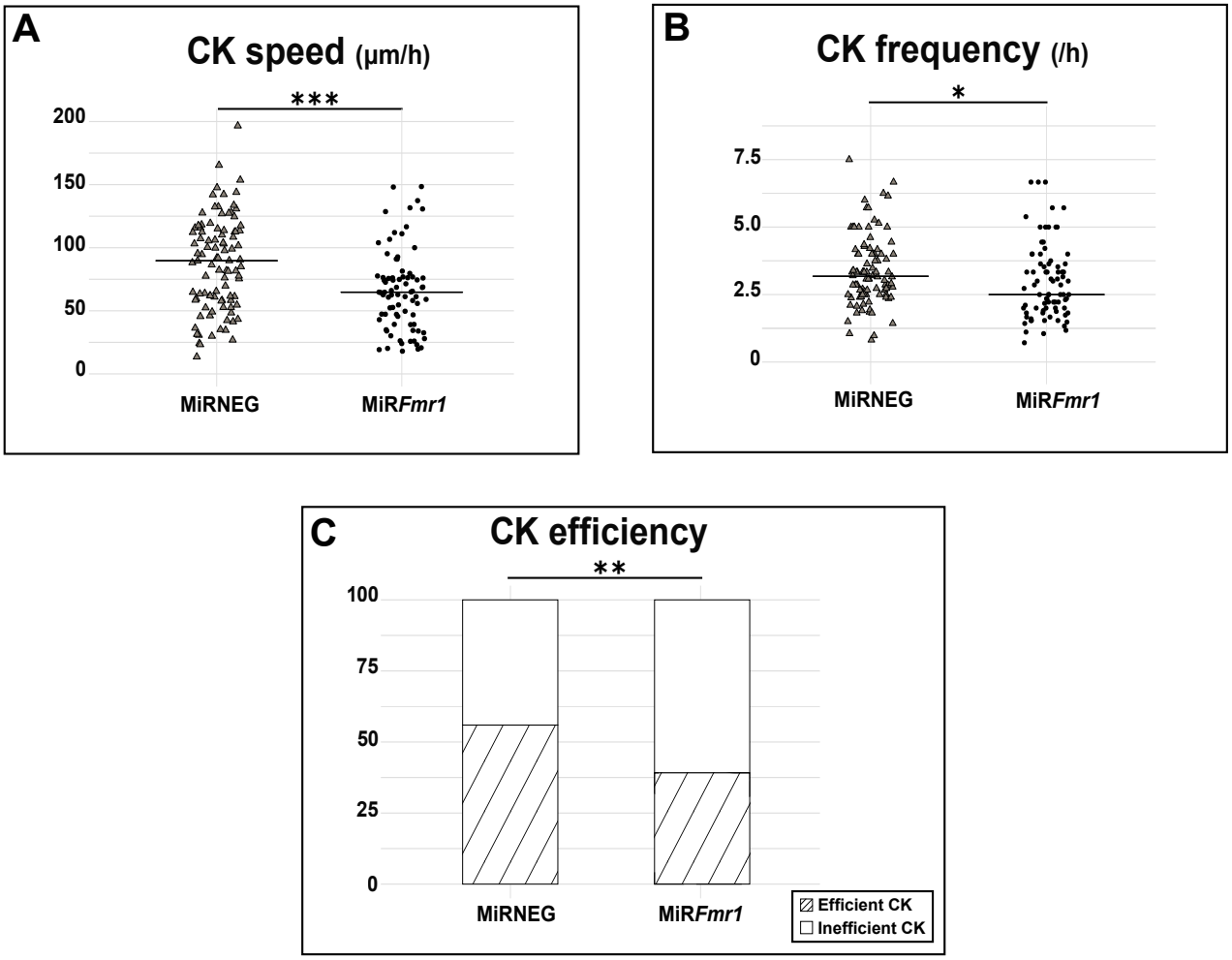

FIGURE 5. ***Fmr1 KD recapitulates Fmr1-null neurons CK defects.*** *(A) CK speed of neurons expressing MiRNEG and MiRFmr1. MiRNEG: 87 ± 4 µm/h; MiRFmr1: 66 ± 3 µm/h (Mann-Whitney test, p-value < 0.001). (B) CK frequency of neurons expressing MiRNEG and MiRFmr1. MiRNEG: 3.4 ± 0.1 CK/h; MiRFmr1: 3.0 ± 0.2 CK/h (Mann-Whitney test, p-value = 0.011). (C) Percentage of efficient CKs in neurons expressing MiRNEG and MiRFmr1. MiRNEG: 57 %; MiRFmr1: 41 % (Chi2 = 17.999, p-value = 0.0012). The black line represents the median. MiRNEG: N = 3, n = 96; MiRFmr1: N = 3, n = 81. *p-value < 0.05; **p-value < 0.005; *** p-value < 0.001.*

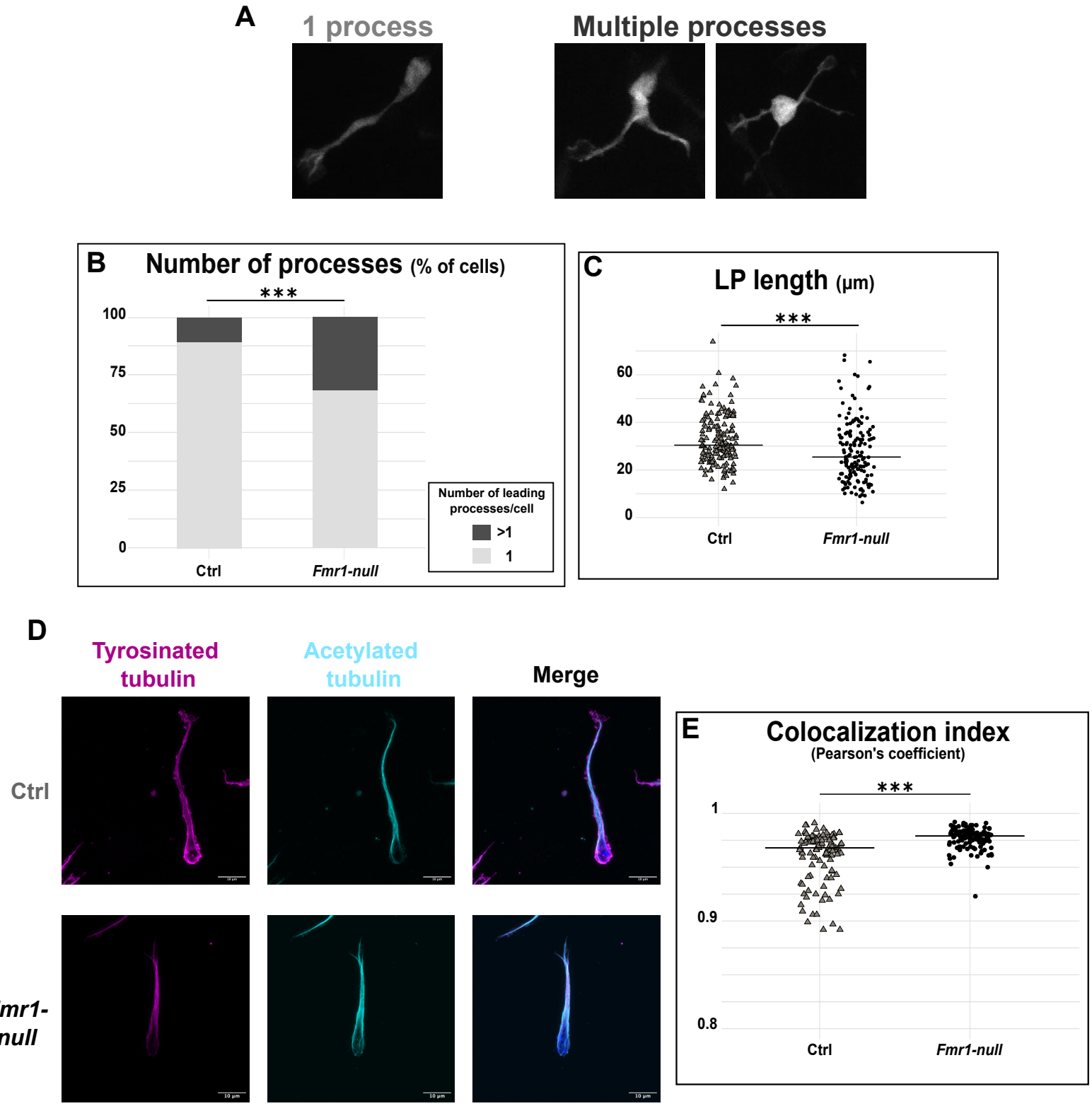

FIGURE 6. ***Fmr1-null neurons exhibit morphological impairments and altered subcellular distribution of tyrosinated MTs.*** *(A) Illustration of RMS-migrating neurons with a unique or multiple process(es). (B) Quantification of the number of processes per cell, depicted as the percentage of cells with a unique or multiple process(es) in control and Fmr1-null neurons. Percentage of neurons with a unique process. Ctrl: 89%; Fmr1-null: 68 %. Percentage of neurons with multiple processes. Ctrl: 11%; Fmr1-null: 32 % (Fisher's Exact test, p-value < 0.001). Ctrl: N = 3, n = 232; Fmr1-null: N = 3, n = 236. (C) Quantification of the leading process' length. Ctrl: 32.4 ± 0.8 µm; Fmr1-null: 27.8 ± 1.0 µm (Mann-Whitney test, p-value < 0.001). Ctrl: N = 3, n = 168; Fmr1-null: N = 3, n = 152. (D) Immunohistochemistry of Fmr1-null and control neurons showing subcellular distribution of tyrosinated tubulin (magenta) and acetylated tubulin (cyan). Scale bar: 10 µm. (E) Quantification of Pearson's coefficient, indicator of colocalization between tyrosinated and acetylated tubulin. Ctrl: 0.960 ± 0.002; Fmr1-null: 0.977 ± 0.001 (Mann-Whitney test, p-value < 0.001). Ctrl: N = 3, n = 107; Fmr1-null: N = 3, n = 122. The black line represents the median. *** p-value < 0.001.*

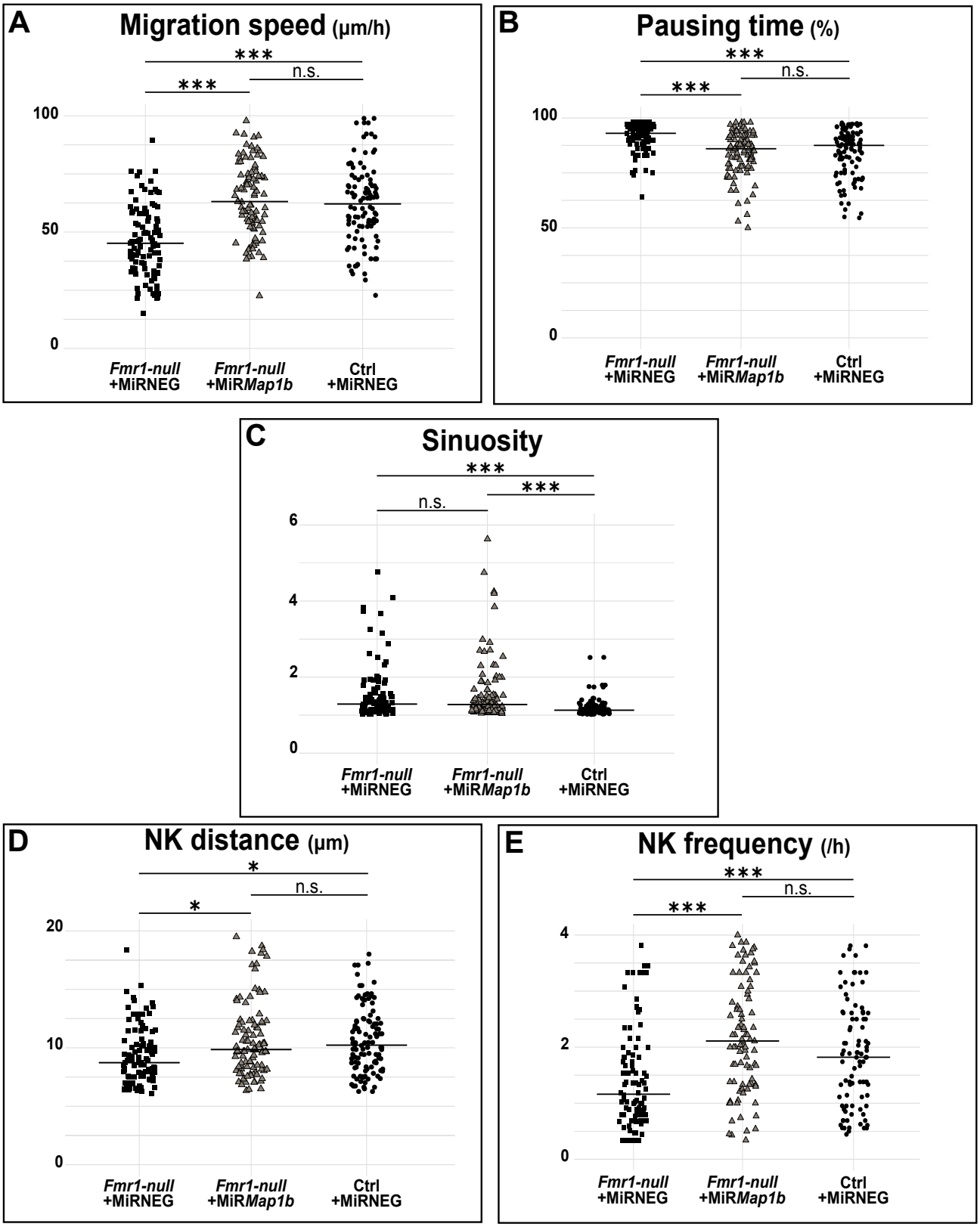

FIGURE 7. *Map1b KD rescues Fmr1-null neurons migration defects.* *(A) Migration speed of Fmr1-null neurons expressing MiRNEG and MiRMap1b and control neurons expressing MiRNEG. Fmr1-null neurons + MiRNEG: 47 ± 2 µm/h; Fmr1-null neurons + MiRMap1b: 67 ± 2 µm/h; control neurons + MiRNEG: 64 ± 2 µm/h (Kruskall-Wallis Test: Chi2 = 61.168, p-value < 0.001, df = 2; followed by Dunn's posthoc test). (B) Percentage of pausing time of Fmr1-null neurons expressing MiRNEG and MiRMap1b and control neurons expressing MiRNEG. Fmr1-null neurons + MiRNEG: 92 %; Fmr1-null neurons + MiRMap1b: 84 %; control neurons + MiRNEG: 84 % (Kruskall-Wallis Test: Chi2 = 45.716, p-value < 0.001, df = 2; followed by Dunn's posthoc test). (C) Sinuosity index of Fmr1-null neurons expressing MiRNEG and MiRMap1b and control neurons expressing MiRNEG. Fmr1-null neurons + MiRNEG: 1.77 ± 0.18; Fmr1-null neurons + MiRMap1b: 1.90 ± 0.20; control neurons + MiRNEG: 1.18 ± 0.02 (Kruskall-Wallis Test: Chi2 = 39.807, p-value < 0.001, df = 2; followed by Dunn's posthoc test). (D) NK mean distance of Fmr1-null neurons expressing MiRNEG and MiRMap1b and control neurons expressing MiRNEG. Fmr1-null neurons + MiRNEG: 9.7 ± 0.3 µm; Fmr1-null neurons + MiRMap1b: 11.1 ± 0.4 µm; control neurons + MiRNEG: 10.6 ± 0.3 µm (Kruskall-Wallis Test: Chi2 = 11.573, p-value = 0.003, df = 2; followed by Dunn's posthoc test). (E) NK frequency of Fmr1-null neurons expressing MiRNEG and MiRMap1b and control neurons expressing MiRNEG. Fmr1-null neurons + MiRNEG: 1.5 ± 0.1 NK/h; Fmr1-null neurons + MiRMap1b: 2.4 ± 0.1 NK/h; control neurons + MiRNEG: 2.5 ± 0.2 NK/h (Kruskall-Wallis Test: Chi2 = 39.272, p-value < 0.001, df = 2; followed by Dunn's posthoc test). The black line represents the median. Fmr1-null neurons + MiRNEG: N = 6, n = 102; Fmr1-null neurons + MiRMap1b: N = 3, n = 101; control neurons + MiRNEG: N = 3, n = 78. * p-value < 0.05; *** p-value < 0.001; n.s. (not significant), p-value > 0.05.*